ELSEVIER

Contents lists available at ScienceDirect

Journal of Hazardous Materials Advances

journal homepage: www.elsevier.com/locate/hazadv





Reusable porous chromium- zinc oxide nano-sheets for efficient detoxification of xenobiotics through integrated advanced oxidation water clean-up process

M. Pavithra, Jessie Raj M B

PG and Research Department of Physics, Bishop Heber College, Affiliated to Bharathidasan University, Tiruchirappalli, Tamil Nadu 620017, India

ARTICLE INFO

Keywords:
Porous Cr-ZnO
AOP process
Type IV hysteresis
Bactericidal
TOC-toxicity assessment

ABSTRACT

An integrated approach of acoustic, ultraviolet, and sunlight-driven Advanced Oxidation Process (AOP) is an excellent choice in the quest for a water-cleaning process. This research delves into the realization of chromiumdoped zinc oxide (Cr/ZnO) nanopores as a low energy, eco-friendly, efficient, and exhibiting stable photocatalysis for the AOP process. Ultrasonic-aided co-precipitation technique was used for the synthesis of porous Cr-ZnO nanostructures. X-ray diffraction patterns and FTIR spectra of the synthesized samples revealed that chromium ions were effectively intruded into the ZnO lattice. Tauc's equation and Kubella Munk plots have explored that the incorporation of Cr dopants in ZnO reduces the optical band energy. The formation of porous structures was evinced in SEM, TEM, HRTEM, and BET studies. The presence of abundant mesoporous structures was confirmed by the adsorption/desorption isotherms of type IV hysteresis. The antimicrobial efficacy of Cr-ZnO against aqueous bacteria, Staphylococcus aureus, and Escherichia coli was comparatively as effective as the control. The integrated AOP approach enhances the electron trapping characteristics of nanoporous Cr-ZnO catalysts to generate self-sustained in-situ reactive oxygen species on the aqueous matrix. In the current research, methylene orange and nitro phenol were detoxified up to 99 % and 98.2 %, and their half-life degradation rate constant was 22 min and 26 min, respectively. The total organic contaminants (TOC) test on the resultant treated water has confirmed the effective detoxification of xenobiotic molecules and the possibility of reusing the treated water. The ecotoxicology research using treated water on flora and primary aquatic microfauna has supported the possibility of practical utilization of Cr-ZnO in harmless environmental adaptation in the foreseeable future.

Introduction

Water is indispensable to living beings. One of the most serious ecological threats we face today is water pollution. In developing countries like India, the production rate of industrial contaminants is increasing steadily every year (Choi et al., 2019). Abundant organic contaminates draining out of the manufacturing sectors have become a prevalent environmental challenge during the last few decades (Das et al., 2020). The effluents not only degrade the water's aesthetic quality but also harm the aquatic vegetation and fauna. There are numerous methods to treat dye-bearing effluents. Despite the availability of many techniques to treat dye contaminants from wastewater, such as chemical oxidation, membrane separation process, electrochemical, adsorption, coagulation/flocculation, precipitation, flotation, ion exchange, ion-pair

extraction, and aerobic and anaerobic microbial degradation, each of these methods have inherent limitations. Such methods may produce new waste that requires additional treatment to be destroyed (Smjecanin et al., August 2022). In the current research, introducing an integrated and innovative trick viz Sono-photo-catalysis (SPC) and advanced oxidation process (AOP) was accompanied by the effective degradation of hazardous azo toxins that must be treated harmlessly before they can be released (Sharifi et al., 2022). Sono-photo-catalysis is a promising approach for the degradation of toxins by the molecular transformation on the surface of the catalyst without leaving a minor pollutant. In this approach, (i) the initial ultra-sonication procedure causes acoustic cavitation in a short amount of time, and generates physical changes in aqueous azo pollutants through a faster chemical reaction; (ii) secondly, UV irradiation treatment improves the

E-mail address: jessie.ph@bhc.edu.in (J.R. M B).

^{*} Corresponding author.

absorption efficiency of photocatalysts, which enhances photocatalytic dye degradation efficacy; and (iii) finally, irradiation under solar light, as a renewable, clean energy source, has a high energy density, and the usage of semiconductor photocatalysts to activate free radicals, have environmental benefits (Naushad et al., 2019). Sunlight-driven AOPs generate in-situ reactive oxygen species (ROS), most notably hydroxyl radicals •OH, ultimately substantiated to have a strategic advantage not only in the treatment of dye effluents but also in the production of energy simultaneously (Shanmugam and Jeyaperumal, 2018).

Nano-photo-catalysts are playing a critical role in the most promising use of solar-powered AOP technology for the treatment of organic contaminants (Mondal et al., 2021). The well-known semiconductor photocatalyst, zinc oxide (ZnO) has the favorable advantages of tuning the band edges, low working temperature, quick electron-hole recombination, inadequate mild absorption, and susceptibility to workable dissolution or photo-dissolution (Kotha et al., 2022). Unfortunately, only (5-7 %) of ultraviolet light can be absorbed by the intrinsic ZnO from the total sunlight, because of its wide band gap, which limits the photocatalytic efficiencies for practical applications (Rekha et al., 2010). It is well known that metal dopants can effectively improve the characteristics of ZnO nanoparticles, and have ample space in the field of research (El-sayed et al., 2022). The doping material should be chosen properly to trigger ZnO photocatalysts for high visible-light-driven photo-activities (AOP) and was done via structural modification and band-gap engineering using Cr dopant ions (Srinet et al., 2020). Chromium is an important transition metal dopant and its ionic radius is close to zinc atoms. As a result, Cr^{3+} ions or Zn^{2+} ions can easily penetrate the ZnO crystal lattice (Br et al., 2023). During the formation of a heterojunction between the doped ion metal (Cr³⁺) and ZnO, cavity traps and collectors have been seen in the Cr-ZnO species. Compared to pure ZnO, Cr-doped ZnO acts as a superior photocatalyst due to its electron trap characteristics. Cr³⁺ dopant ions liberate enormous electrons and convert them into Cr^{2+} ions $(Cr^{3+} + e^{-} \rightarrow Cr^{2+})$, thus electron trapping occurs in the ZnO matrix (Gürbüz and Okutan, 2016). The electron trapping process reduces the recombination rate of electron-hole pairs and generates in-situ reactive oxygen species to destroy the organic compounds in the aqueous matrix. Thus, chromium doped in ZnO contributes to high degradation efficiency.

Various synthesis methods including chemical vapor deposition (Nguyen et al., 2022), spray pyrolysis, microwave assist (Qamar et al., 2022), sol-gel, co-precipitation, and hydrothermal method (Ulfa et al., 2023; El Messaoudi et al., 2022) are used for the preparation of Cr-doped ZnO nanoparticles (Mohamed et al., 2021). In the present work, Cr-doped ZnO nanoparticles were prepared successfully by the ultra-sonication-aided co-precipitation method (Chen et al., 2020). As synthesized, Cr-ZnO nano powders were characterised using X-ray diffractometer (XRD), FT-infrared spectrometer, ultraviolet (UV) visible and UV-diffused reflectance spectrophotometer, dynamic light scattering (DLS), photoluminescence (PL), scanning electron microscope (SEM), tunnelling electron microscope (TEM and HRTEM), and Brunauer-Emmett-Teller (BET) analysis.

The proficiency of photocatalytic degradability of Cr-doped ZnO nanostructures to detoxify the widely used anionic azo dyes, methyl orange (MO) and nitro phenol (4-NP) were analysed. These xenobiotics are environmentally and biologically hazardous, therefore, so they are to be treated harmlessly before they can be released (Shah et al., 2021). Antibacterial properties, total organic carbon (TOC) test, and toxicity test using flora and microfauna were assessed for environmental protection (Liu et al., 2020).

Experimental procedure

Preparation of self-assembled porous Cr-ZnO nanosheets

Cr-doped ZnO nanoporous structures developed by ultrasonicassisted co-precipitation technique. According to the literature, ultrasonic-assisted preparation results in greater photocatalytic efficacies than traditional approaches for the breakdown of azo toxins (Sadeghi Rad et al., 2022). The reagent-grade chemicals of chromium (III)acetate, zinc acetate dihydrate, and sodium hydroxide from Sigma-Aldrich, India were utilized in the synthesis procedure (Li et al., 2018). The aqueous solution of zinc acetate (0.97/0.95 M), chromium acetate (0.03/0.05 M), and sodium hydroxide (2 M) was made using ultrapure de-ionized water (Milli-Q-Millipore). Homogeneous mixing of chromium acetate with zinc acetate solution was done by steady magnetic stirring (Bodke et al., 2015). Following that, sodium hydroxide was slowly added to the precursor solution and agitated for 3 h. The nucleation process and formation of the nanostructure were improved by sonication of the resultant solution for 1 h. The powder precipitate was desiccated at room temperature, calcined at 350 °C for 2 h, and after being washed with ethanol (Pavithra and Jessie Raj, 2021). A schematic diagram for the preparatory steps of Cr-ZnO products is shown in Fig 0.1

Sono-photocatalytic detoxification process (SPC)

The degradation of aqueous MO/NP pollutants was assessed by measuring them spectrophotometrically. In the present work, the dye concentration of 3×10^{-6} mol/L was treated with 0.03 g/L of Cr-ZnO catalyst in the optimized pH - 7.2 at room temperature (Alkallas et al., 2022). The mixture was ultra-sonicated and UV light irradiated for half an hour in the dark before exposing it to sunlight. The ultra-sonication and UV irradiation measure adopted in the current research is the tricky key role, which prompts the establishment of adsorption-desorption equilibrium and dispersion of Cr-doped ZnO nano photocatalysts of fine particles. Then the mixture was kept under sunlight illumination and the degradation capability of Cr-doped ZnO catalysis was estimated by finding absorbance with the help of a UV–Vis spectrometer(Shimadzu/UV-2600) (Paustian et al., 2022).

Inactivation of Bacteria in the aqueous environment

Staphylococcus aureus-902 and Escherichia-443 are unicellular organisms, lined in the aqueous environment. The interaction of microorganisms with nano-sized Cr-doped ZnO nanoparticles was determined against these test pathogens by the zone inhibition method. Petri plates containing 20 ml of nutritional growth media were seeded with bacterial strains that had been incubated for 24 h at 37 $^{\circ}\text{C}$ (Pavithra and Jessie Raj, 2022). Wells were cut and various concentrations of sample zinc oxide and Cr-doped ZnO (3 %, and 5 %) were injected. The diameter of the inhibition zone created around the wells was obtained by measuring the bacterial inactivation effect. As a positive control, the antibiotic gentamicin was utilized (Pneumonia et al., 2020).

Phytotoxicity analysis using treated water

Phytotoxicity analysis is a useful tool to determine the Cr-ZnO sample's suitability after potential treatment and reuse of effluent water for real-time utility (Nguyen et al., 2021). The toxic effect of dyes mixed with water and treated water was investigated using germination of *Vigna Radiata* seeds. More or less uniform-sized, healthy *Vigna Radiata* seeds were chosen and to remove adherent impurities, washed 3–4 times with double distilled water and incubated in double distilled water overnight to soften the stiff seed coat. The Petri dish cultivation method was adopted to find out the germination percentage and development of seedlings. For the greatest growth, the Petri plates were kept dark and warm for 5 to 7 days (Worku et al., 2021). The experiment was performed with distilled water as a control and photocatalytic dye-degraded water and the response of cultivars was recorded. These tests were performed in triplicate to improve consistency.

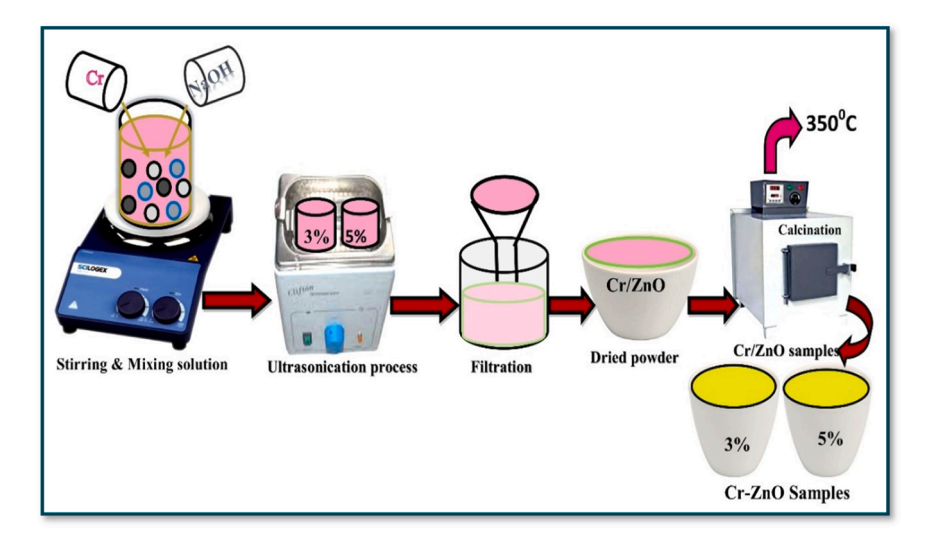


Fig. 1. Schematic explores the process of precursor solution preparation, ultra-sonication, filtration, precipitation, and calcination to synthesize Cr-ZnO samples.

Survival assessment of Artemia cysts in treated water

Artemia (Brine shrimp) are small aquatic crustaceans. Moreover, it can be easily cultured and has a short life cycle. The chosen subspecies of Artemia for this research work is its nauplii, a smaller kind of Artemia than Artemia salina. Toxicological results may be determined by the organism's life phases as well as the test settings in the lab. The cysts, dried eggs with a hatchability of 99 %, were purchased from the aquarium fishery department, near the harbour in Thoothkuti, Tamil Nadu, India, and the cysts were kept in an airtight glass vial in a humid environment. As part of the continuing investigation, a tiny pinch of cysts was initially placed in a vesicle filled with sterilized synthetic saltwater at ambient temperature with continual oxygenation. The beaker was kept under white light (Philips, bulb F8T5) and maintained at room temperature (20 ±5 °C). The Artemia was hatched overnight (24 to 36 h) and then twenty nauplii were transferred into four 500 mL vessels using a pipette (Tapia-Salazar et al., 2022). It was aimed at estimating the survival amount of Artemia per container. After the start of exposure, lethality assessment was done by use of a light microscope (model: LABOMED SP. ACHRO with magnification 10x / 0.25, 40x / 0.65, 100x/1.25) at every six-hour intervals of treatment (from 6 to 54 h). Artemia salina nauplii's activity was photographed and recorded with a smartphone camera (OPPO F9 Pro). Toxicity of aqua media and survival assessment was done by analysing the nauplii's activities at regular intervals.

Results and discussion

Bragg diffraction patterns of self-assembled porous Cr-ZnO nanosheets

The two-step processing procedure via co-precipitation, followed by an acoustic irradiation approach has a substantial impact on the crystallinity of the material for developing self-assembled Cr-ZnO nanopores. Also, it is feasible to intrude chromium ions at Zn locations in the crystalline matrix by reducing the specific surface area of the materials. Powder X-ray diffraction (PXRD) profiles expressed in Fig.2 have clearly shown that the diffraction peaks are highly crystalline, well-defined and the addition of a few Cr ions has almost no effect on the fundamental crystal structure of ZnO (Naz and Saeed, 2021). The output confirming chromium ions were uniformly diffused into the lattice of ZnO. The predicted miller indices of PXRD patterns revealed that the lattice planes are standard diffraction patterns of hexagonal wurtzite zinc oxide crystalline phase (JCPDS No. 36–1451), namely., (100), (002), (101), (102), (110), (103), (200), (112), and (201) crystal planes. No secondary

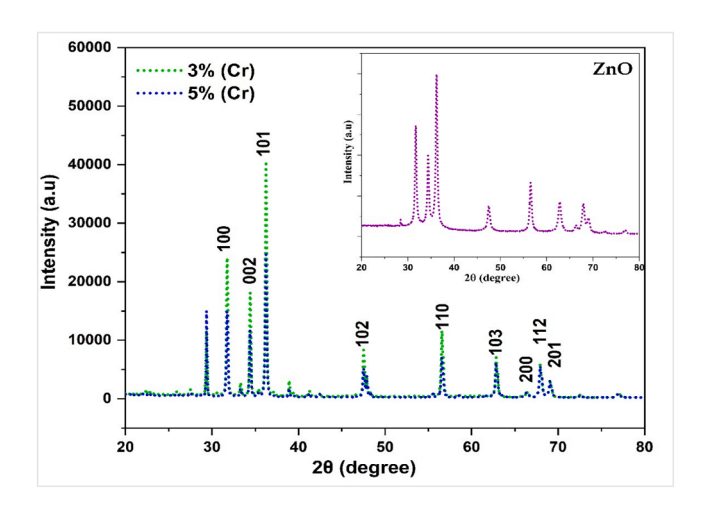


Fig. 2. Powder XRD profiles of self-assembled porous Cr-ZnO nanosheets (inset: pure ZnO), indicating characteristic peaks and Miller planes.

phases in PXRD analysis were observed, indicating that Cr ion substitution did not affect the wurtzite structure (Iqbal et al., 2020a).

But by increasing Cr doping, there is a slight broadening of full width at half-maximum [FWHM], decrement in intensity, and negligible angle shift in diffraction peaks were highlighted in their successful incorporation. Due to the introduction of Cr ions into the Zn lattice, the in-plane atomic arrangement with closed atomic packing could be strained. Besides that, the geometrical structure of the ZnO was altered because of the slight difference in the ionic radii between Cr (0.63 Å) and Zn (0.74 Å), and the transport of materials takes place mostly by volume diffusion of atoms and ions (Nguyen et al., 2019a). Volume diffusion proceeds either by an interstitial or by a vacancy mechanism. The grain boundaries in the agglomerate are constrained and the nanopores are created due to the intragranular porosity and the grains. Thus, the lattice strain and dislocation density are expected to increase with the increase of Cr content. PXRD results exemplified though the addition of Cr retaining ZnO structure, the crystallite size, microstrain, and dislocation density of ZnO nanoparticles has a minor effect and the readings were tabulated in

In the present study, the inter-granular porosity depends on chromium concentration and grain growth. The porosity increases with the substituent concentration of Cr (3 % to 5 % variation) in ZnO. An intraband transition of the Cr-3d bands occurs with the (CB) conduction

Table 1PXRD data to find Crystallite size, Micro strain and Dislocation density of Cr-ZnO samples.

Samples	Bragg's angle 2θ (degree)	FWHM β (degree)	d-spacing (*10 ⁻¹⁰ m)	Crystallite size (*10 ⁻⁹ m)	Micro strain (*10 ⁻⁴ a.u)	Dislocation density (*10 ¹⁴ lines/m²)
5 % Cr in ZnO	36.23	0.19	2.477	43.9	7.88	5.16
3 % Cr in ZnO	36.21	0.17	2.478	47	7.35	4.49

band, resulting in a prominent region of visible light absorption of the solar radiation and hence enhancing the photocatalytic action.

Vibrational frequencies of self-assembled porous Cr-ZnO nanosheets

The vibrational behaviour of the functional groups which are presented in the prepared Cr-doped porous ZnO nanosheets was inspected by FTIR analysis in the wave number range from 4000 to 400 cm⁻¹. The transmittance FTIR spectra of wurtzite Cr-ZnO nanostructures were explored in Fig 3. FTIR peak is positioned at $439~{\rm cm}^{-1}$ related to the lattice oxygen and metal (Zn-O) bond and at 650 $\,$ cm⁻¹ could be assigned to O—Cr-O bonding (Mahesha et al., 2023). The FTIR spectrum associated with the metal-oxygen bond in 5 % Cr-ZnO was broadened at these frequencies compared to 3 % Cr-ZnO. This result demonstrated the lattice distortion in metal-oxygen bonding due to the presence of Cr-ion doping. The increased intensity in the FTIR spectrum of 5 % Cr-ZnO depicts the successful doping of Cr ions in the ZnO matrix (Iqbal et al., 2020b). Stretching modes of Zn-O-Cr were observed between 821 cm⁻¹ and 946 cm⁻¹, confirming the presence of defects caused by oxygen vacancies in the system due to Cr incorporation in the ZnO lattice, which matches the previous literature (Altuner et al., 2023). A deep and sharper band around 1381 cm⁻¹ and a band at 1095 cm⁻¹ are assigned to the stretching vibrations of Zn-Cr and Cr-O bonds, respectively (Devi et al., 2021). Bending vibration H—O-H is observed near 1631 cm⁻¹ due to the small amount of water adsorbed on the surface of as-prepared Cr-ZnO nanoparticles. The broad absorption bands around the range 3450 cm⁻¹ are due to the deconvoluted hydroxyl bonding (-OH) of surface adsorbed water in the Zn-O lattice (Shohany and Zak, 2020). Thus, FTIR analysis revealed the Cr ion was developed and incorporated into the ZnO lattice as evidenced by the XRD measurement results.

Optical properties of self-assembled porous Cr-ZnO nanosheets

UV–Vis spectra of Cr-ZnO nanosheets are shown in inset Fig 4(a). The linear optical characteristics of Cr-ZnO exemplify a significant small shift and sharp absorption band edge, such as the increase of Cr^{3+} ions into the ZnO matrix (Khan et al., 2021). The shift is due to the

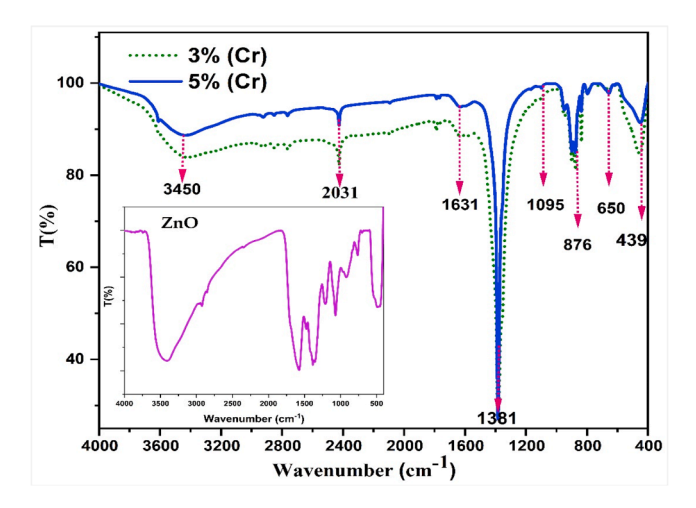


Fig. 3. Fourier Transform Infrared spectra displaying characteristic vibrational frequencies of (inset: pure ZnO) porous Cr-ZnO nanosheets.

ultra-sonication which produces ${\rm Cr}^{3+}$ ions with more dynamic deformity locales in the ZnO lattice or spin-correlated exciton formation or to crystal de-formation through doping. Strong visible-light absorption was found in Cr- ZnO via active defect sites owing to s-d and p-d exchange interactions between conduction electrons and localized d electrons of chromium ions. Also, the results of 5 % Cr doping in ZnO lead to more absorption than 3 % Cr-ZnO nanostructures, indicating that its optical capability is nearly in the visible range. A greater number of ${\rm Cr}^{3+}$ ions are substituted in the zinc ion lattice for creating more active sites, improving the surface charge of ZnO, and is favourable for improved photocatalytic and bacterial control (Qamar et al., 2020).

Tauc's plot has been used to determine the band gap energy of Cr-ZnO nanoparticles. The optical energy band gap of pure ZnO is 3.2 eV (Pavithra and Jessie Raj, 2022), However, after injecting chromium into the zinc oxide, it drops from 2.95 eV to 2.87 eV, shown in inset Fig.4(b). Trapping of chromium atoms at the grain boundaries leads to the formation of defect sites within the forbidden band (Qamar et al., 2020). The band gap energy of the Cr-doped samples was reduced due to the electronic structure modification and quantum size impact. The lower band gap energy of Cr-doped ZnO nanoparticles relies on a larger grain boundary density. By increasing the chromium doping concentration, the density of these defect sites increases, thus decreasing the band gap. Tuning the energy band gap by Cr doping in the ZnO matrix makes it capable of controlling pathogens and the degradation of pollutants.

Ultraviolet-visible diffuse reflectance spectroscopy was also used to analyse the linear optical characteristics of Cr-doped ZnO nanoparticles. 5 % Cr doping in ZnO leads to more absorption than 3 % Cr-ZnO nanostructures as in Fig 4, indicating that improved surface charge of ZnO. The higher electronic population during the 5 % Cr doping in ZnO leads to the quantum confinement effect and blue shift in optical absorption behaviour. Trapping of chromium atoms at the grain boundaries leads to the formation of defect sites within the forbidden band, creating the sub-energy level in ZnO between the conduction and valance bands. This leads to visible light absorption in Cr-doped ZnO nanoparticles. The incorporation of Cr ions into the ZnO lattice changes the electronic level, reducing the optical energy band gap and boosting the light absorption capability. For band gap calculations, the Kebula Munk factor, $F(R)^2$ was plotted as the function of energy (Qamar et al., 2020). It was found that the band gap of Cr- ZnO nanostructures decreased from 2.5 eV to 2.4 eV with increasing the incorporated Cr content from 3 % to 5 %. The band gap energy of the Cr-doped nanoparticles was reduced due to the electronic structure modification and quantum size impact. Cr-doped ZnO nanoparticles have a lower band gap energy due to a larger grain boundary density. The results were comparable to the band gap obtained from Tauc's plot.

The photoluminescence study was carried out at an excitation wavelength of 325 nm at room temperature. Prominent PL emission peaks of Cr-ZnO in Fig 4(c) were found around 384–387 nm, which arise from the recombination of free excitons and are generally assigned as a near-band-edge (NBE) emission band. More electrons were induced by chromium dopants, taking up the energy levels at the valence band in Cr-doped ZnO nanoparticles and the excited electrons occupy greater energy levels at the bottom of the conduction band, resulting in the radioactive recombination of these excitons (Rupa et al., 2019). The band gap moves slightly towards blue due to the lattice strain generated by the lattice distance and at least some Cr ions are integrated into the ZnO lattice sites. Profound level luminescence has lately been attributed to two separate defect origins, the oxygen vacancy, and the zinc

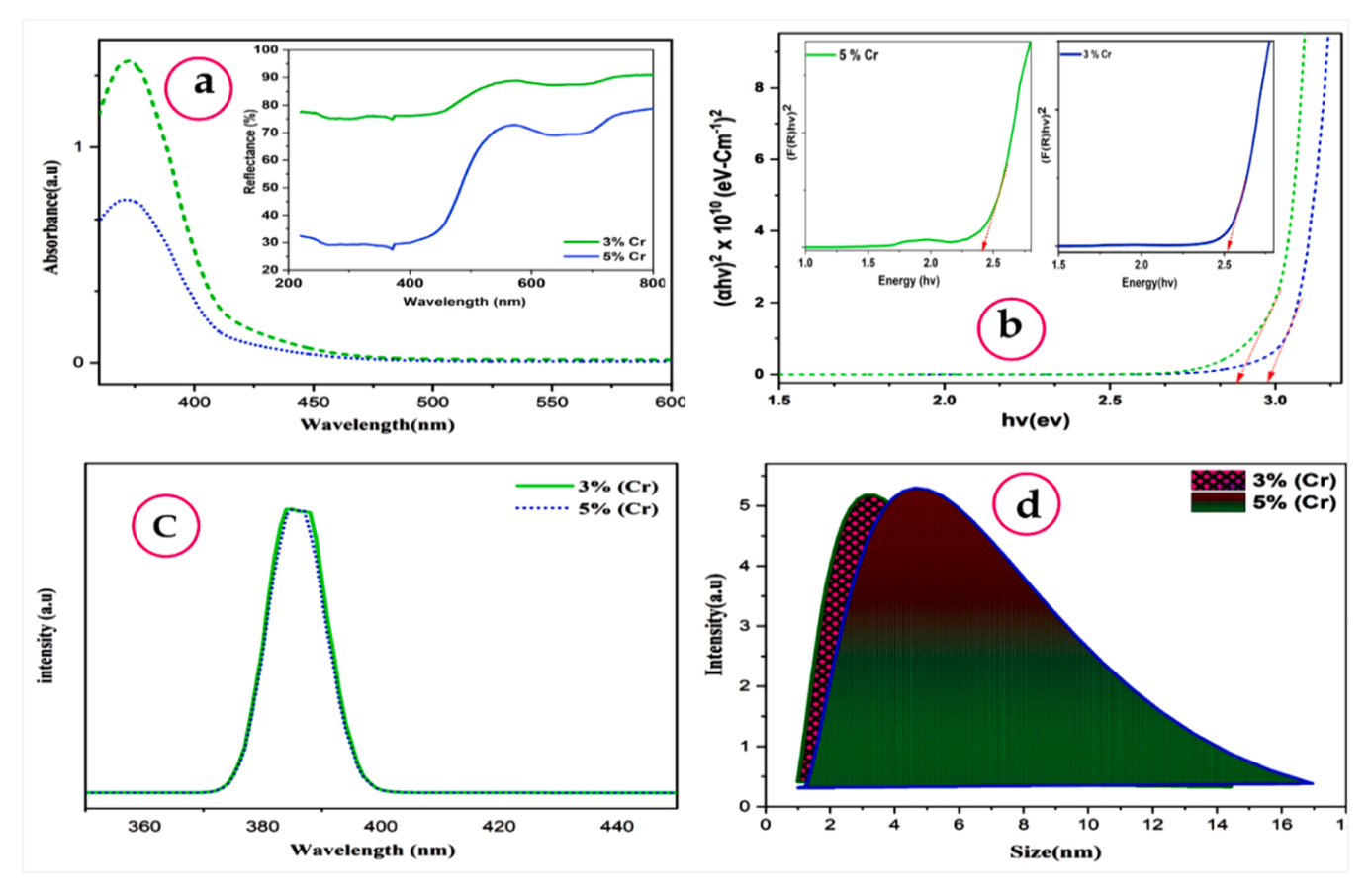


Fig. 4. Optical properties of Cr-ZnO: (a) UV- Vis absorbance spectra (inset-UV-DRS spectra), (b) Tauc's plots (inset-Kebelka -Munk plots), (c) PL spectra, and (d) DLS distribution plots.

vacancy, both of which have different optical properties. Cr-doping effectively inhibits this component emission in the present condition. It is revealed that some Cr dopants may also take the place of Zn vacancy, which can increase the defects and oxygen vacancies in ZnO (Khayyami et al., 2020). Photoluminescence (PL) spectra results illustrated that a well-defined hierarchical porous structure is particularly

desired for the low recombination rate of carriers. Further, based on the nanosheets assembled hierarchical structure, which showed more outstanding photocatalytic behaviour with high degradation capability for MO and 4-NP under sunlight irradiation (Nguyen et al., 2019b).

Dynamic light scattering technique was used to estimate the mean aggregate size of the Cr-ZnO nanoporous materials (Mahdavi et al.,

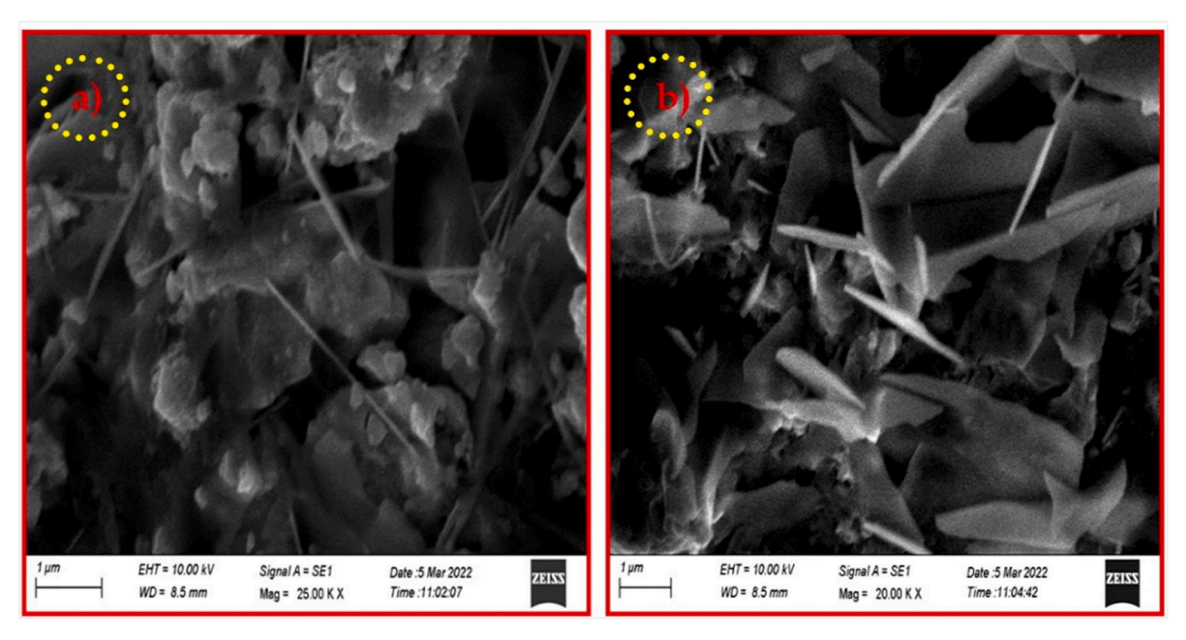


Fig. 5. Surface morphology of (a) 3 % Cr and (b) 5 % Cr-doped ZnO nanosheets, displaying the formation of self-assembled porous networks.

2021). The DLS distribution plot of Fig 4.d illustrates scatter in the range of (1 to 17 nm) with a mean colloidal size of 6.5 nm and a standard deviation of 1.5 nm. The observations shows that a smaller particle size distribution was produced when the amount of Cr in ZnO was increased. This reduction in particle size is due to the distortion in the host material incorporated with a greater number of chromium ions in the ZnO nanoparticle's surface area. Hence, it enters into the bacteria without much strain and is also suitable for degradation of MO/4-NP contaminants.

Morphology of Cr-ZnO nanoporous networks

The self-assembled chromium-doped zinc oxide nanosheets explored an entirely different porous surface morphology, as in the SEM images of Fig 5. This nano porosity shape was attributed to the effective substitution of Cr³⁺ doping ions into zinc oxide lattice, arranged as petals/sheets-like nano porosity networks with tapering ends, though they appear to be broadly agglomerated. The morphology of nanoparticles depends on the value of the ionic fraction of the chromium–zinc bonding (Huang et al., 2021). The electronegativity of zinc is 1.65 on the Pauling scale, while that of chromium is 1.66 on the same scale, i.e., the ionic fraction is low. Further, an increase in the electronegativity of the chromium dopant element can change the porous structure. A more interconnected porous distribution was obtained at 5 % Cr-ZnO than at 3 % Cr-ZnO. This indicates that the morphology of the parent compound was altered by the doping element.

As a result, dopant-Cr³⁺ acted as a structure-directing agent during formation (Gomez-Polo et al., 2021). The increased surface area of assembled nanosheets and the formation of rectangular tubular structures, as well as the abundance of basal edges can result in a more active

response to the strong visible-light absorption ability. These irregular nanosheets assembled due to the weak interactions make tubular-tunnel-like structures. With the increase of Cr ions in ZnO, oxygen vacancies and defect sites render multimode voids between and within the porous nanosheets, extending the light response range to induce better photocatalytic activity.

The elemental composition of the Cr-ZnO samples was identified with energy-dispersive spectroscopy (EDS) (Khayyami et al., 2020). Elemental analysis (EDS) of the Cr-ZnO nano porous sample showed absorption peaks of Cr, Zn, and O with a weight percentage of 0.6, 83.1, and 16.3, as shown in Fig 6. There are no additional peaks observed indicating the high purity level of the synthesized sample.

TEM and HRTEM were employed to study the porous morphology of Cr-doped ZnO nanocomposites and the selected area electron diffraction (SAED) was done to confirm the crystal planes of the Cr-ZnO sample. The bright spots seen in TEM predicted the sample's high crystallinity (Valerio et al., 2019). The concentric rings of the SAED pattern have been matched with (100), (002), (101), (102), (110), and (200) the crystal planes as shown in Fig.6(a) and (b), revealing the growth of wurtzite structure of crystalline chromium doped Zinc oxide. The examination of crystal lattice planes, d spacing, and particle distribution was analysed using Image J software. The presence of porous structures in TEM analysis is consistent with SEM. HRTEM images clearly showed lattice fringes without defects indicating a high degree of crystallinity (Tangcharoen, 2023). HRTEM images reveal their structures as highly crystalline twin structures, and their d-spacing distances at 0.265 nm correspond to the (002) plane and 0.239 nm correspond to (101) the highest plane (El-sayed et al., 2022). The outcome is similar to that of XRD which proved the wurtzite phase of Cr ions doped in the ZnO lattice (Wu et al., 2011).

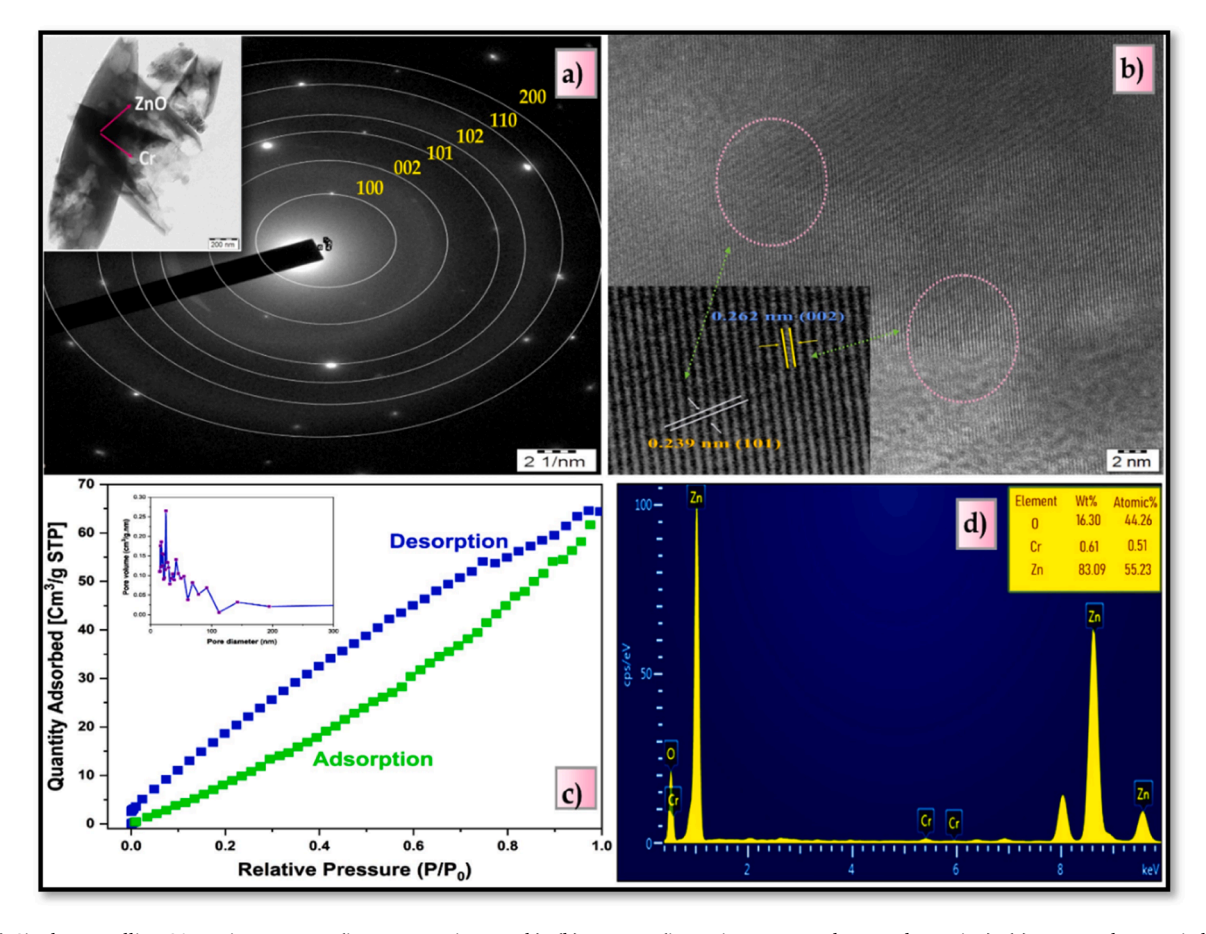


Fig. 6. (a) Single crystalline SAED rings pattern (inset-TEM micrograph), (b) HRTEM (inset- inverse FFT denotes d- spacing), (c) Type IV hysteresis loop of BET isotherms (inset-pore size distribution), and (d) EDX analysis (inset- elemental composition) of Cr- doped porous ZnO nanosheets.

Brunauer-Emmett-Teller (BET) analysis was performed to find out about the surface area, pore size distribution, and pore volume of the Cr-ZnO nano porous sample. The nitrogen adsorption-desorption isotherms for Cr-ZnO nanopores along with the Barrett-Joyner-Halenda (BJH model) were presented in Fig.6. C. The N2 adsorption-desorption isotherms of Cr-ZnO belong to typical type IV isotherms with an obvious hysteresis loop (relative Pressure in the range (0.1–1.0), portraying the mesoporous nature (Manohar et al., 2023). From BET, the surface area was found to be 61.633 m 2 g $^{-1}$. This observation was further substantiated by the pore size distribution curve in Fig 6. Based on the BJH model, the pore volume of Cr-ZnO NPs was found to be 0.104 cm³/g. Moreover, the pore size distribution is mainly concentrated between 10 and 40 nm, which is caused by the cavity formed by petal-like networks of Cr-ZnO stacking together, which is consistent with SEM and TEM analysis. Thus, the significant surface area and pore volume could provide more active sites, shorten the transporting path of ions on the surface, and facilitate better photocatalytic activity.

Antibacterial activity of porous Cr-ZnO nanosheets

The antibacterial response of ZnO and Cr-ZnO porous nanosheets was assessed against therapeutically extracted bacteria *Staphylococcus aureus*(*G*+) and *Escherichia coli* (*G*-) which are usually seen in polluted aqueous media and normally found in the stomach of healthy humans and animals. Cr-doped ZnO was tested against these bacterial strains by well diffusion assessment (Rayani Nivethitha and Carolin Jeniba Rachel, 2019).

Pathogen inactivation during the water remediation process was prompted by the ROS-inspired antibacterial strategy via advanced oxidation redox technology that generates highly reactive oxygen species. Chromium-doped zinc oxide is an active, self-regenerating catalyst and has a promising possibility as an effective antibacterial agent due to its ability to start generating reactive oxygen species and their powerful oxidizing superoxide, less toxic reactive oxygen species radicals ['O2], hydrogen peroxide [H₂O₂], and reactive hydroxyl radicals ['OH] that enter cells, inhibit the antioxidant defence system, inhibit ATP production, degrade bacterial integrity, and cause structural damage to the cell membrane. ROS damages the cellular protein molecules and deoxyribonucleic acid, causing cell death (Yan et al., 2023). The schematic representation of eradicating bacterial organisms is shown in Fig 0.7.

ZnO nanoparticles have the inherent ability to induce ROS production with extreme chemical activity, leading to apoptosis. Besides, cell damage is mediated by ROS generated on the surface of ZnO after photocatalysis by subsequently absorbing surface oxygen to form ROS, electrons can be quickly transferred between Cr ions and ZnO nanoparticles, and hence chromium ion dopants in ZnO serve as a photocatalytic antibacterial agent. The ROS of Cr-ZnO survives long enough to diffuse into bacterial species (Ikram et al., 2023). Cr-ZnO nanostructures bind with the cell membrane of bacteria and the probability of photo-generated electron–hole pair recombination is reduced as a result of the trapping of electrons by chromium ions, where chromium in more reactive oxygen species is produced (Elamin et al., 2021). ROS reactive oxygen generation causes oxidative stress and the mechanism of bacteria's intracellular region is disturbed. The inactivation of protein

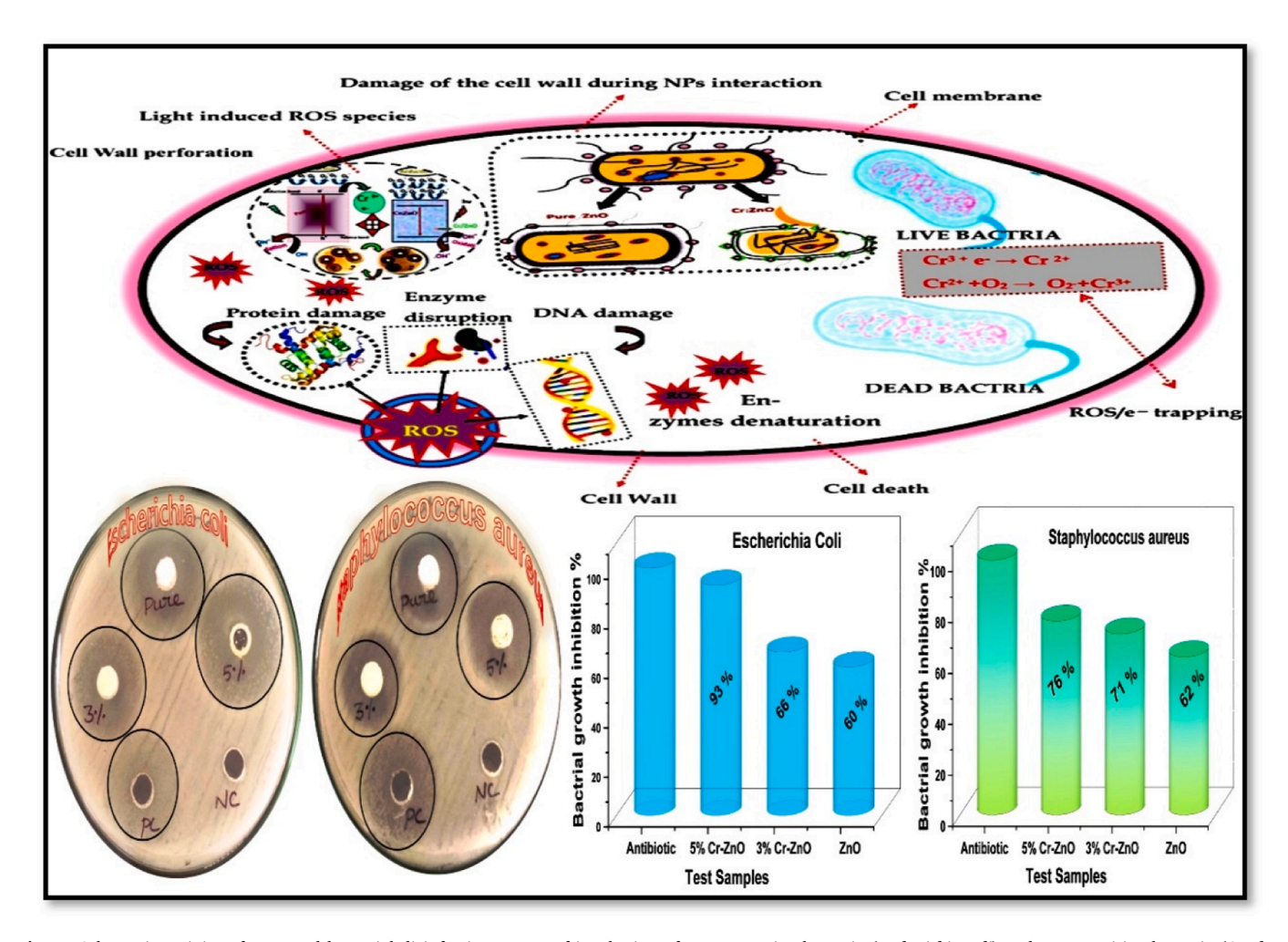


Fig. 7. Schematic activity of proposed bacterial disinfection, Zones of incubation of gram-negative bacteria (Escherichia coli) and gram-positive bacteria (Staphylococcus aureus), and comparative plots of percentage of bacterial growth inhibition against pure and Cr-doped ZnO samples.

molecules is triggered by Cr-ZnO nanoparticles, which reduces the permeability of the cell membrane. More chromium ions are diffused into cellular membranes, due to the high affinity of ${\rm Cr}^{3+}$ ions for phosphates, which are abundant in the DNA molecule, and prompt inhibition of the pathogenic bacteria membrane's surface and altering its barrier properties, ultimately causing substantial cell damage (Rao and Shekhawat, 2014) Thus, chromium and zinc ions released from the Cr-ZnO enter into the cell wall, causing DNA, protein, and mitochondrial damage as well as an interruption in electron transport, leading to cell death.

As soon as the positive control on the bacterial cells on the surface of the medium begins, the creation and growth of inhibition zones are visible. Antibacterial responses increase with the reduction in the dimension of nanopores. Inhibition zone diameters are measured in mm and are tabulated in Table 2. According to the present findings, 5 % Cr-ZnO nanosheets have a better antibacterial effect (Ren et al., 2021). The percentage of bacterial inhibition of Staphylococcus aureus (G+) and E. Coli(G-) versus the composition of samples were shown in the comparative plot in Fig 7. The key role of ZnO in ROS exhibited mortality rates against E. coli and S. aureus depending on the concentration of the dopant and nanopore size The zones of inhibition of 5 % Cr-ZnO against S. aureus were found to be as effective (23.1 \pm 1.41 mm) as antigen (23.5 \pm 0.7 mm) and for *E. coli* were found to be superior (30.05 ± 0.5 mm) than antigen (18.2 \pm 0.28 mm). The result depicted that Cr-doped ZnO nanocomposites explore a better antibacterial effect as compared to antibiotics.

Integrated AOP-Sono photocatalytic detoxification of azo contaminants

Intending to remove drastically polluting xenobiotic compounds present in aquatic habitats and resolve the present serious environmental issues, properly chosen and perfectly designed nano photocatalysts are promising materials due to their ability to use advanced oxidation species via solar light to kindle photocatalytic reactions (Amir et al., 2022).

• Photocatalytic mechanism

The mechanism for enhancing the photocatalytic activity of heterogeneous ${\rm Cr}^{3+}$ - ZnO was proposed concerning point defect evolution through the manner of ${\rm Cr}^{3+}$ doping. The doped ${\rm Cr}^{3+}$ ion acts as an electron trap in the ZnO crystal. In this respect, an atomic-level interpretation of the photocatalytic mechanism of Cr-doped ZnO materials would be highly demanded. The cavity traps and collectors have been seen in the Cr-ZnO species (Sachin et al., 2023). The electron trapping process reduced the recombination rate of electron–hole pairs, which resulted in the improvement of the photocatalytic performance.

In the present study, Cr-ZnO possesses high photocatalytic performance because of increased sunlight harvesting, well-separated reductive and oxidative active sites, generation of reactive oxygen species (ROS), and strong redox ability. Under AOP, electrons in the valence band (VB) will be excited to higher levels called electron-trapped centres, which are from native or impurity-induced defects whose levels lie in the band gap. The excitation process could repeat several times to bring a valence electron to the CB to be a free electron and simultaneously leave a hole in the VB. The excited electron in the conduction

Table 2Zones of inhibition (mm) showing the antibacterial potential of Cr-ZnO samples.

Name of the test	Inhibition zone diameter (mm)			
organism	Pure ZnO	3 % Cr doped ZnO	5 % Cr doped ZnO	control
Staphylococcus aureus	18.5 ± 0.7	21.25 ± 0.35	23.1 ± 1.41	23.5 ± 0.7
E. coli	$\begin{array}{c} 18.2 \pm \\ 0.28 \end{array}$	20.6 ± 0.14	30.05 ± 0.07	$\begin{array}{c} 24.5 \; \pm \\ 0.7 \end{array}$

band (CB) could be trapped by a Cr^{3+} ion to reduce this ion to a lower oxidation state, Cr^{2+} . Then Cr^{2+} ions will react with O_2 in the solution to form superoxide radicals. The better photocatalytic activity performance outcome could be understood as reflecting the formation of a heterojunction between the doped ion metal (Cr^{3+}) and ZnO, which reduced the radiative recombination rate, thus exciting the photoelectron, and the hole gained a longer lifetime to react with organic compounds in the solution regime. This contributes to the observed high degradation efficiency. The combined advanced oxidation process (AOP) is prompt to detoxify methyl orange and phenolic compounds in water (Joshi et al., 2020). As a result, azo dyes were adsorbed on the photocatalyst's surface.

The degree of degradation of azo toxins versus concentration was estimated using a UV-spectrophotometer (Keerthana et al., 2021). The schematic of the photocatalytic mechanism for treating MO and 4-NP mixed wastewater by self-sensitization using Cr-ZnO porous nanosheets in combined acoustic-UV- solar irradiated and the advanced oxidation process is shown in Fig.8. MO and 4-NP were gradually degraded by Cr-ZnO nanopores due to the generation of strong oxidative radicals in the coactive process as follows (Álvarez et al., 2020).

 $Cr - ZnOPhotocatalysts + hv(directsunlight) \rightarrow$

$$Cr(e^{-})$$
(conductionband, CB)+ $ZnO(h^{+})$ (valanceband, VB) (1)

$$Cr(e^{-})$$
conductionband $+ O_2 \rightarrow Cr + O_2^{\bullet -}$. (2)

$$O_2^{\bullet^-} + 2Cr(e^-) + 2H^+ \to OH^{\bullet} + OH^-.$$
 (3)

$$ZnO(h^+)$$
valenceband + $H_2O \rightarrow OH^{\bullet}$. (4)

$$MO/4 - NP$$
contaminants $+ ZnO(h^+)VB \rightarrow Oxidation products$ (5)

$$MO/4 - NP$$
contaminants $+ Cr(e^{-})CB \rightarrow Oxidation products$ (6)

Radicals $(OH^{\bullet}orO_{2}^{\bullet})$ + organic molecules \rightarrow intermediates \rightarrow Degradation products (7)

• Degradation efficiency

The molecules of MO and 4-NP were degraded by Cr-ZnO up to 99 % and 98.2 % respectively. The phenol and methyl orange absorption spectrum almost vanished after 120 min of solar light irradiation, indicating that the toxic components were constantly destroyed (Pavithra et al., Nov 2023).

The intensity of the distinctive peaks of intermediates (P-benzoquinone, C-catechol, and H-hydroquinone) declined, indicating that they were degraded to $\rm CO_2$ and $\rm H_2O$ (Kumar et al., 2021). A putative methyl orange and phenol degradation pathway by chromium-doped zinc oxide was postulated based on the analysis of intermediates, as illustrated in Fig.9.C.

• Kinetic model

The pseudo-first-order kinetic plotting indicates the photo-degradation of contaminants fits well with the kinetic model. The linear plots with high $\rm R^2$ values (more than 0.9) for MO and 4-NP degradation using Cr/ZnO, supported that the degradation of the pollutants obeys first-order reaction kinetics. Fig. 9b has confirmed that pseudo-first-order rate constants of MO and 4-NP pollutants are 0.0307 min⁻¹ and 0.0263 min⁻¹ respectively (Riaz et al., 2020).

• Photocatalytic performance

The optimal photocatalytic performance of Cr-doped ZnO catalysts was determined by (C/C_0) plots for the photodegradation of MO and 4-

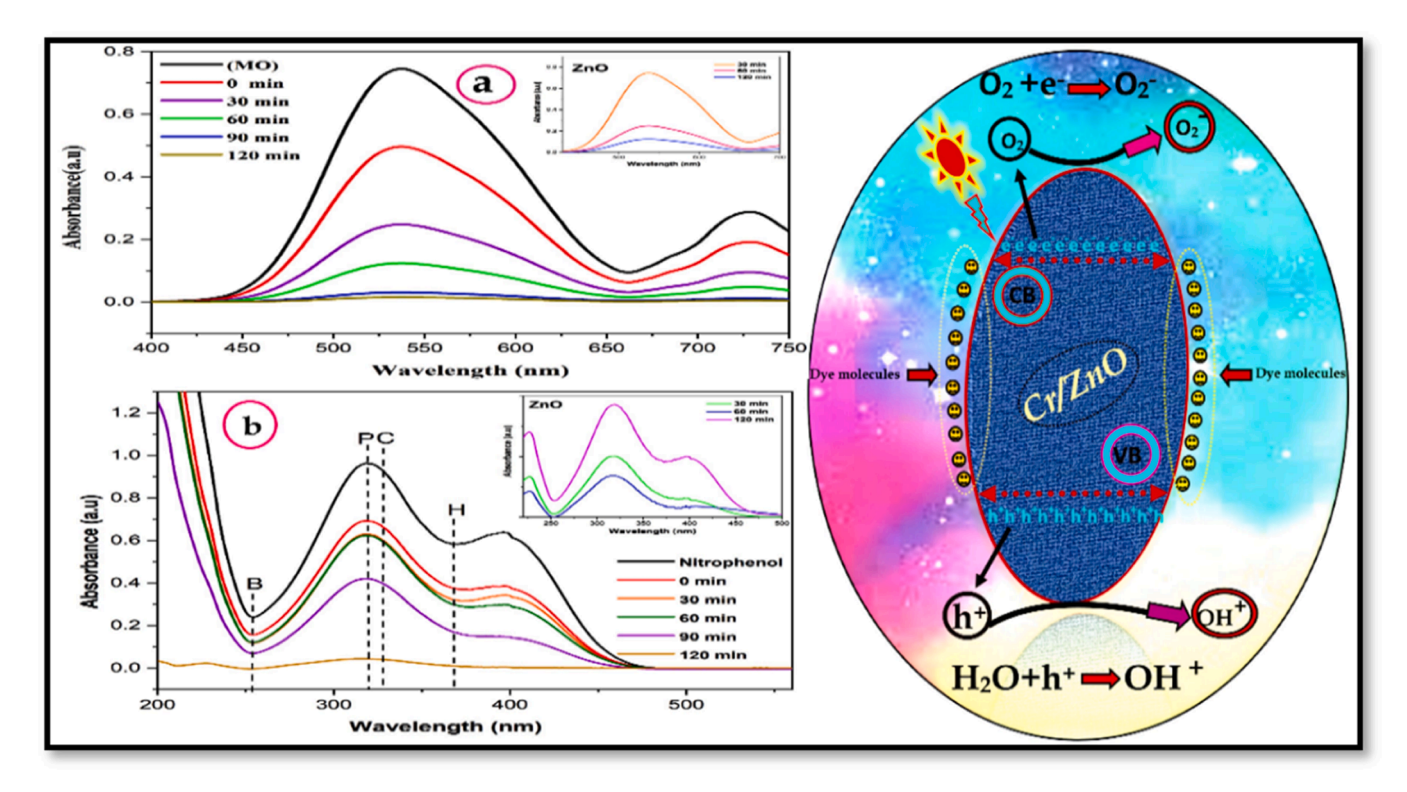


Fig. 8. Photocatalytic degradation plots of (a) methylene orange (b) phenol effluents using Cr-doped ZnO nanopores by AOP process in the period of 0 to 120 min (inset -decomposition of azo dyes using pure ZnO) and (c) the possible photocatalytic pathway.

NP contaminants, as shown in Fig. 8. The half-life of the reaction was calculated using the formula,

$$\mathbf{R}_{1/2} = \mathbf{ln2/K} \tag{8}$$

Here, $R_{1/2}$ is half-life of reaction, and K is the rate constant. The values of the rate constant disclosing the half-life of reaction for MO and 4-NP pollutants are 22 min and 26 min, respectively.

· Stability and reusability

After the reaction is completed, Cr-ZnO is separated by simple centrifugation, dried at room temperature, and analysed for the possibility of recycling used samples for further degradation of xenobiotic contaminants Fig.9d (Anju et al., 2012). The photocatalytic degradability of Cr-ZnO nano-catalyst retains its stability up to four cycles and hence implies its possibility of re-usage, which further recommended that Cr-ZnO might be suitable alternate and powerful photocatalysts for degrading hazardous MO and NP organic molecules.

• TOC analysis

The presence of total organic carbon (TOC) after the treatment of MO and 4-NP xenobiotics in the aqueous solution was also studied by a TOC analyser (Model: TOC-LCPN SHIMADZU). The results of the TOC test showed that toxic carbon organic bonds were greatly decreased and broken into harmless molecules (Wu et al., 2011). The mean value of TOC for MO-treated water is 60.97 % and for 4-NP is 75.33 %. Thus, the Cr-ZnO nano-photocatalysts is a suitable candidate for decomposing MO and 4-NP from an aqueous solution.

• Electrical energy per order (EEO) evaluation

At ground level, 44 % of the sunlight energy is in the visible range, with only 3 % in the ultraviolet range. Complete usage of UV light is often the indispensable light source in the photocatalytic system to

activate the photocatalytic degradation of pollutants, but unavoidably increases the cost and operation difficulties. This work aimed to investigate the feasibility of using Cr-ZnO for dye decomposition by initial exposure of acoustic and UV for adsorption and desorption dark equilibrium, then under sunlight as a green technology.

Photocatalytic degradation of organic pollutants follows pseudofirst-order kinetics and is connected to electrical energy (Mohagheghian et al., 2015). Electrical energy per order (EEO) is the figure-of-merit, determines the electrical energy cost evaluation, and predicts the suitability of the Cr-doped ZnO catalyst in AOP for wastewater treatment. The kinetic model, based on the initial rates of degradation, provided a good prediction of the EEO values.

Decomposition of methylene orange (MO)/nitrophenol (4-NP) was done by exposing pollutant-containing water to ultrasonic/UV light (20 W) for 20 min and then under sunlight illumination of approximately 83,000 Lux (656 W per second during solar noon, exposed at $10^{\circ}48'52''N$, $78^{\circ}40'22''E$ - Bishop Heber College, Tiruchirappalli, Tamil Nadu, India) for 120 min.

The equation for the determination of EEO (Lee et al., 2018),

$$EEO \left(KW \, \big/ \, m^3 \, \, \big/ \, per \; order \right) \; = \; \frac{E \, \times \, t \, \times \, 1000}{V \, \times \, 60 \, \times \, log \left(\frac{C_c}{C_f}\right)}$$

where P is the power (kW), t is the treatment time (min), V is the volume of the reactor (L), and k is the pseudo-first-order rate constant (min⁻¹) for the deterioration of the pollutant concentration. The EEO results show that 5 % Cr-doped ZnO nanostructures are energy-saving photocatalysts (455 KW/m³ for MO and 596 KW/m³ for 4NP) than pure ZnO (1535 KW/m³ for MO and 2721 KW/m³ for 4NP) by AOP. It is revealed that the energy demand for photocatalytic xenobiotic degradation was drastically reduced when Cr-doped ZnO hybrid nanostructures were used in comparison to pure ZnO catalysts (Elbadawy et al., 2023). Thus, eco-friendly and freely available solar-driven AOPs in the utilization of the Cr-doped ZnO catalysts efficiently reduce electrical energy consumption.

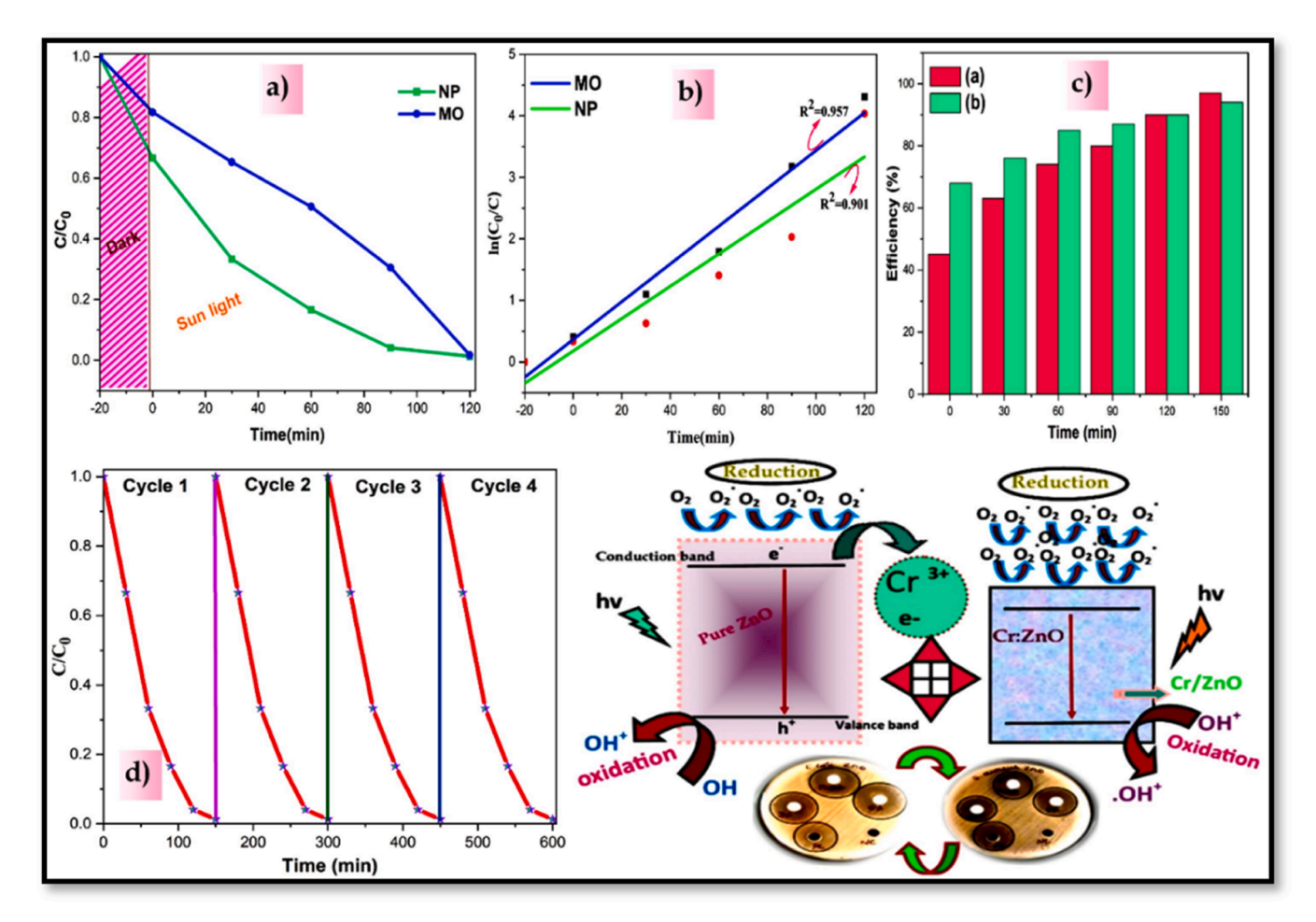


Fig. 9. Mitigation of xenobiotic compounds (a) photocatalytic degradation plots, (b) corresponding pseudo-first-order kinetic plots, (c) toxins removal Efficiency, (d) stability and reusability of Cr-ZnO samples, and (e) schematic of self-generating ROS in Cr-ZnO than pure ZnO and photo reduction activity by AOP.

Plant nanotoxicity of treated water

The basic components of all ecosystems are plants. It is an important precondition for promoting Cr-ZnO in real-time photocatalytic applications and avoiding potential ecological risks (Dsikowitzky and Schwarzbauer, 2014). Hence, the prospects of research put forward in the direction of phytotoxicity analysis, an indispensable aspect of risk assessment, and help to understand the interaction between detoxified water and plants. Seeds imbibe more water during the development of seed coat and so plant nanotoxicity studies have chosen to determine the inhibition of treated water in plant species, green grams (*Vigna radiata*). Several aspects of plant growth were analysed including seed germination and shoot development.

The experiment revealed that the germination percentage of *Vigna radiata* seeds in distilled water as control (100 %), untreated dye solution was almost terminated (2 %) and grew better in photocatalytic-treated dye-containing water (90 \pm 5 %). It is evident that Vigna radiata seeds in distilled water and treated water have high seed viability and germination percentages were comparable. The germination of seeds was prohibited in dye-containing water (2 %) due to toxicity. The seedling Vigor index was almost zero in dye-containing water, indicating the low concentration of toxins can affect the seed's growth and vice versa.

Further, the well-grown seed amongst the ten seeds was replaced in test tubes and tested for plant growth in 5 days as shown in Fig.10 (Jayarambabu et al., 2014). Enhancive and inhibitive effects of treated water on plants' growth have been documented in Table 3. After the degradation of xenobiotic MO and 4-NP contaminants in wastewater

using Cr-ZnO nanocatalysts, the treated water showed low biological toxicity and harmless environmental behaviour. Thus, it is predicted that the toxicity of the dye-containing solution was reduced after being treated with the Cr-doped ZnO catalyst as shown in Fig. 10, and provided logical solutions to the ecological challenges of detoxifying effluents.

Acute toxicity of treated water

The direct potential toxicity of pollutant-treated exposure media to aquatic organisms was examined by analysing the survival rate of nauplii of *Artemia salina* in treated water. Twenty highly mobile nauplii were selected and put in an oxygenated tank with treated water (Svensson et al., 2005). The toxicological results were determined by documenting the organism's life phases of the hatched nauplii of *Artemia* brine shrimp in treated water media. The experiment was repeated three times and the persistence of *Artemia* nauplii groups in the photocatalysts degraded water was compared to the control group (Danabas et al., 2020). The outcome showed the usage of treated water in a small aquatic *Artemia salina* model as shown in Fig.11 poses low toxicity risks. The observations were statistically significant, and predicted that Cr-ZnO is one of the best detoxifiers and reuse of effluent water in an eco-friendly manner.

Conclusion

The formation of self-assembled porous Cr-ZnO nanosheets was synthesized by the ultrasonic-co-precipitation method. Chromium dopant acts as a structure-directing agent for the synergetic altering of

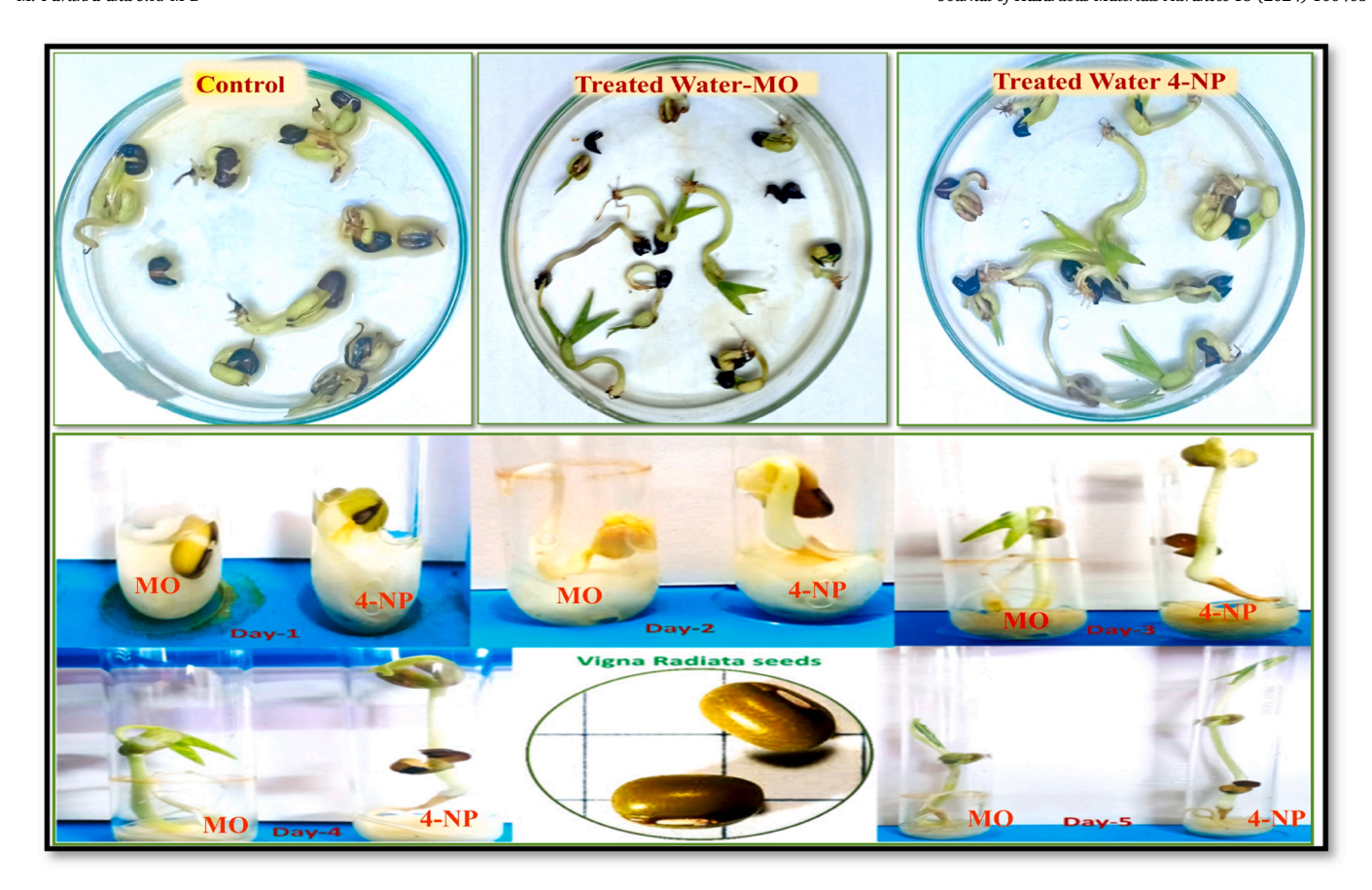


Fig. 10. a) Germination of Vigna radiata Seeds in control and treated water and (b) Plant nano toxicity analysis by growth of Vigna radiata plants for 5 days after germination, at room temperature.

 $\begin{tabular}{ll} \textbf{Table 3} \\ \textbf{Seed germination, seed vigor index, and plant nanotoxicity assessment using } \\ \textit{Vigna radiata seedlings in the treated water.} \\ \end{tabular}$

Parameters	Plant growth (shoot length) in triplicate measurements $(mean \pm SD \ in \ cm)$				
	Treated water (Methylene orange)	Treated w (Nitro phe			
Day 1	0.3 ± 0.5	0.5 ± 0	.5		
Day 2	0.8 ± 0.3	1.3 ± 0	1.3 ± 0.4		
Day 3	1.3 ± 0.2	2.2 ± 0.2			
Day 4	1.9 ± 0.4	2.8 ± 0.3			
Day 5	2.4 ± 0.5	3.2 ± 0.5			
	Control	Treated	Treated water		
		MO	4-NP		
Germination (%)	100	90	95		
Seed Vigor Index 1500		1243	1406		

the porous size of ZnO structures. PXRD, FT-IR, UV, PL, SEM, TEM, DLS, BET, and TOC studies were carried out to describe the development of Cr-ZnO as a promising Sono-photo catalyst. Under the integrated AOP approach of the ultrasonic-catalytic process under sunlight irradiation, Cr-ZnO obeys first-order reaction kinetics and is proficient for methyl orange and phenol degradation. The xenobiotics (MO and 4-NP pollutants) have almost vanished (above 90 %) after 120 min of exposure, and the rate constants at the half-life of the reaction were 22 min and 26 min, respectively. Further, Cr-ZnO plays a vital role in easily restricting aquatic pathogens, feasible for plant metabolism and natural aquatic microfauna. Thus, the current research hopes to bring new ideas for the reuse of treated industrial wastewater in a sustainable, safe environment and emerge into the green revolution soon.

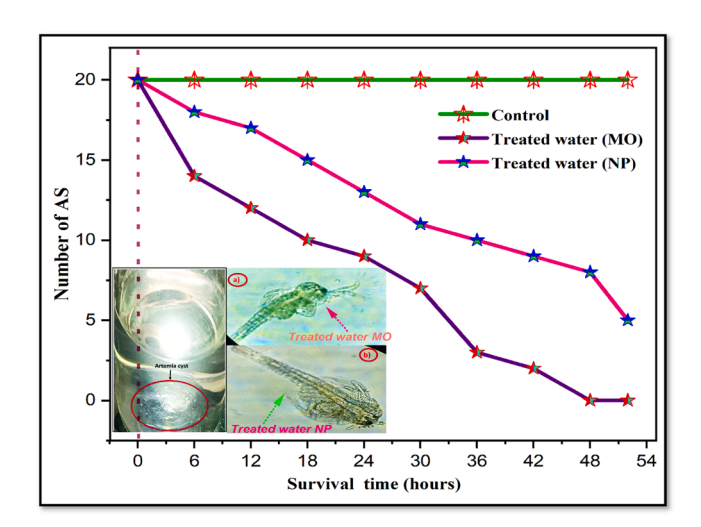


Fig. 11. Treated water-control versus survival rate of *Artemia salina* (AS) comparative plots to find acute toxicity of treated water (inset image cysts development and survival of AS).

Conflict of interest

The authors declare that they have no conflict of interest.

Novelty statement

With the ever-increasing demand for clean energy and water, it's no wonder that photocatalysis is a hotly debated topic. So, this is an

important area for researchers working on the synthesis of new low-energy photocatalysts for the mitigation of contaminants. The state-of-the-art self-assembling networks of chromium-zinc oxide nano-sheets to form mesoporous structures exhibit electron trap characteristics under an integrated advanced oxidation process (AOP) to stimulate and destroy the organic contaminant molecules on the surface of the catalyst by self-generating free radicals in aqueous media. The supreme degradation efficiency of Cr-ZnO explores further utilization of the resultant treated water ensuring less toxicity to flora, primary aquatic consumers microfauna, and for the prevalence of natural aquatic ecosystems.

Funding

The authors declare that no funds, grants, or other support were received during the preparation of this manuscript.

CRediT authorship contribution statement

M. Pavithra: Data curation, Formal analysis, Writing – original draft. **Jessie Raj M B:** Conceptualization, Formal analysis, Project administration, Supervision, Validation, Writing – review & editing.

Declaration of competing interest

The authors declare that they have no known competing financial interests or personal relationships that could have appeared to influence the work reported in this paper.

Data availability

Data will be made available on request.

Acknowledgment

The authors would like to thank Bishop Heber College, Tiruchirappalli, Tamil Nadu, India for the support given to carry out this research work.

References

- Alkallas, F.H., et al., 2022. Promising Cr-doped ZnO Nanorods for photocatalytic degradation facing pollution. Appl. Sci. 12 (1) https://doi.org/10.3390/ appl.2010034
- Altuner, E.E., et al., 2023. Highly efficient palladium-zinc oxide nanoparticles synthesized by biogenic methods: characterization, hydrogen production and photocatalytic activities. Chem. Eng. J. Adv. 14, 100465 https://doi.org/10.1016/j. ceia.2023.100465.
- Álvarez, M.A., et al., 2020. Removal of parabens from water by UV-driven advanced oxidation processes. Chem. Eng. J. 379, 122334 https://doi.org/10.1016/j. cei.2019.122334.
- Amir, M., et al., 2022. Integrated adsorptive and photocatalytic degradation of pharmaceutical micropollutant, ciprofloxacin employing biochar-ZnO composite photocatalysts. J. Ind. Eng. Chem. 115, 171–182. https://doi.org/10.1016/j. iiec.2022.07.050.
- Anju, S.G., et al., 2012. Zinc oxide mediated sonophotocatalytic degradation of phenol in water. Chem. Eng. J. 189–190, 84–93. https://doi.org/10.1016/j.cej.2012.02.032.
- Bodke, M., et al., 2015. Synthesis and characterization of chromium doped zinc sulfide nanoparticles. OALib 02 (05), 1–8. https://doi.org/10.4236/oalib.1101549.
- Br, S., et al., 2023. Cr (VI) removal from aqueous solution using modified zeolite-iron chloride and its future recommendation. Inorg. Chem. Commun. 157, 111273 https://doi.org/10.1016/j.inoche.2023.111273.
- Chen, J., et al., 2020. Insight into the synergistic effect of adsorption-photocatalysis for the removal of organic dye pollutants by Cr-doped ZnO. Langmuir 36 (2), 520–533. https://doi.org/10.1021/acs.langmuir.9b02879.
- Choi, Y.K., et al., 2019. Investigations on the ZnO- and Cr-doped ZnO powders. Bull. Mater. Sci. 42 (4) https://doi.org/10.1007/s12034-019-1832-2.
- Danabas, D., et al., 2020. Effects of Zn and ZnO nanoparticles on Artemia salina and Daphnia magna organisms: toxicity, accumulation and elimination. Sci. Total Environ. 711, 134869 https://doi.org/10.1016/j.scitotenv.2019.134869.
- Das, A., et al., 2020. Mn-doped ZnO:role of morphological evolution on enhanced photocatalytic performance. Energy Reports 6, 737–741. https://doi.org/10.1016/j. egyr.2019.11.148.

- Devi, K.N., et al., 2021. Nickel doped zinc oxide with improved photocatalytic activity for malachite green dye degradation and parameters affecting the degradation. J. Mater. Sci. Mater. Electron. 32 (7), 8733–8745. https://doi.org/10.1007/s10854-021.05545-x
- Dsikowitzky, L., Schwarzbauer, J., 2014. Industrial organic contaminants: identification, toxicity and fate in the environment. Environ. Chem. Lett. 12 (3), 371–386. https://doi.org/10.1007/s10311-014-0467-1.
- El Messaoudi, N., et al., 2022. Hydrothermally engineered Eriobotrya japonica leaves/ MgO nanocomposites with potential applications in wastewater treatment. Groundw. Sustain. Dev. 16, 100728 https://doi.org/10.1016/j.gsd.2022.100728.
- El-sayed, H.M., et al., 2022. Versatile eco-friendly electrochemical sensor based on chromium-doped zinc oxide nanoparticles for determination of safinamide aided by green assessment criteria. Microchem. J. 182, 107900 https://doi.org/10.1016/j. microc.2022.107900.
- Elamin, N., Modwi, A., Aissa, M.A.B., Taha, K.K., Al-Duaij, O.K., Yousef, T.A., 2021. Fabrication of Cr–ZnO photocatalyst by starch-assisted sol–gel method for photodegradation of congo red under visible light. J. Mater. Sci. Mater. Electron. 32 (2), 2234–2248. https://doi.org/10.1007/s10854-020-04988-y.
- Elbadawy, H.A., et al., 2023. Sustainable and energy-efficient photocatalytic degradation of textile dye assisted by ecofriendly synthesized silver nanoparticles. Sci. Rep. 13 (1), 1–13. https://doi.org/10.1038/s41598-023-29507-x.
- Gürbüz, Osman, Okutan, Mustafa, 2016. Structural, electrical, and dielectric properties of Cr doped ZnO thin films: role of Cr concentration. Appl. Surf. Sci. 387, 1211–1218. https://doi.org/10.1016/j.apsusc.2016.06.114.
- Gomez-Polo, C., et al., 2021. Improved photocatalytic and antibacterial performance of Cr doped TiO2 nanoparticles. Surf. Interfaces 22, 100867. https://doi.org/10.1016/ j.surfin.2020.100867.
- Huang, Wugen, et al., 2021. Atomic structures and electronic properties of Cr-doped ZnO (1010)) surfaces. Chin. J. Catal. 42 (6), 971–979. https://doi.org/10.1016/S1872-2067(20)63710-X.
- Ikram, M., et al., 2023. Toward efficient bactericidal and dye degradation performance of strontium- and starch-doped Fe2O3 nanostructures: in silico molecular docking studies. ACS Omega 8 (8), 8066–8077. https://doi.org/10.1021/acsomega.2c07980.
- Iqbal, M., et al., 2020a. Facile synthesis of Cr doped hierarchical ZnO nano-structures for enhanced photovoltaic performance. Inorg. Chem. Commun. 116, 107902 https:// doi.org/10.1016/j.inoche.2020.107902.
- Iqbal, J., et al., 2020b. Facile green synthesis approach for the production of chromium oxide nanoparticles and their different in vitro biological activities. Microsc. Res. Tech. 83 (6), 706–719. https://doi.org/10.1002/jemt.23460.
- Jayarambabu, N., et al., 2014. Germination and growth characteristics of mungbean seeds (Vigna radiata L.) affected by synthesized zinc oxide nanoparticles. Int. J. Curr. Eng. Technol. 4 (5), 3411–3416. http://inpressco.com/category/ijcet.
- Joshi, N.C., et al., 2020. Antibacterial activity, characterizations, and biological synthesis of manganese oxide nanoparticles using the extract of Aloe vera. Asian Pacific J. Heal. Sci. 7 (3), 27–29. https://doi.org/10.21276/apjhs.2020.7.3.7.
- Keerthana, S.P., et al., 2021. A strategy to enhance the photocatalytic efficiency of α-Fe2O3. Chemosphere 270. https://doi.org/10.1016/j.chemosphere.2020.129498
- Khan, M.I., et al., 2021. Investigation of in-vitro antibacterial and seed germination properties of green synthesized pure and nickel doped ZnO nanoparticles. Phys. B Condens. Matter 601, 412563. https://doi.org/10.1016/j.physb.2020.412563.
- Khayyami, D., et al., 2020. The investigation of Amido black 10B adsorption-photocatalytic degradation using the synergistic effect of Cr-doped ZnO/CDs nanocomposite under solar light. Environ. Sci. Pollut. Res. 27 (8), 8759–8771. https://doi.org/10.1007/s11356-019-07564-y.
- Kotha, V., et al., 2022. Doping with chemically hard elements to improve photocatalytic properties of ZnO nanostructures. J. Clust. Sci. 33 (5), 1943–1950. https://doi.org/ 10.1007/s10876-021-02115-3.
- Kumar, R., et al., 2021. ZnO–SnO2 nanocubes for fluorescence sensing and dye degradation applications. Ceram. Int. 47 (5), 6201–6210. https://doi.org/10.1016/j. ceramint.2020.10.198.
- Lee, C.G., et al., 2018. Porous electrospun fibers embedding TiO2 for adsorption and photocatalytic degradation of water pollutants. Environ. Sci. Technol. 52 (7), 4285–4293. https://doi.org/10.1021/acs.est.7b06508.
- Li, Z., et al., 2018. One step synthesis of Co/Cr-codoped ZnO nanoparticle with superb adsorption properties for various anionic organic pollutants and its regeneration. J. Hazard. Mater. 352, 204–214. https://doi.org/10.1016/j.jhazmat.2018.03.049.
- Liu, J., et al., 2020. Superoxide anion: critical source of high performance antibacterial activity in Co-Doped ZnO QDs. Ceram. Int. 46 (10), 15822–15830. https://doi.org/10.1016/j.ceramint.2020.03.129.
- Mahdavi, V., et al., 2021. Aminoguanidine modified magnetic graphene oxide as a robust nanoadsorbent for efficient removal and extraction of chlorpyrifos residue from water. J. Environ. Chem. Eng. 9 (5), 106117 https://doi.org/10.1016/j. jece.2021.106117.
- Mahesha, A., et al., 2023. Chromium-doped ZnO nanoparticles synthesized via auto-combustion: evaluation of concentration-dependent structural, band gap-narrowing effect, luminescence properties and photocatalytic activity. Ceram. Int. 49 (14), 22890–22901. https://doi.org/10.1016/j.ceramint.2023.04.113.
- Manohar, A., et al., 2023. Structural, BET and EPR properties of mixed zinc-manganese spinel ferrites nanoparticles for energy storage applications. Ceram. Int. 49 (12), 19717–19727. https://doi.org/10.1016/j.ceramint.2023.03.089.
- Mohagheghian, A., et al., 2015. Photocatalytic degradation of a textile dye by illuminated tungsten oxide nanopowder. J. Adv. Oxid. Technol. 18 (1), 61–68. https://doi.org/10.1515/jaots-2015-0108.
- Mohamed, R.M., et al., 2021. A novel design of porous Cr2O3@ZnO nanocomposites as highly efficient photocatalyst toward degradation of antibiotics: a case study of

- ciprofloxacin. Sep. Purif. Technol. 266, 118588 https://doi.org/10.1016/j.
- Mondal, S., et al., 2021. Defect-rich, negatively-charged SnS2 nanosheets for efficient photocatalytic Cr(VI) reduction and organic dye adsorption in water. J. Colloid Interface Sci. 603, 110–119. https://doi.org/10.1016/j.jcis.2021.06.092.
- Naushad, M., et al., 2019. Adsorption kinetics, isotherm and reusability studies for the removal of cationic dye from aqueous medium using arginine modified activated carbon. J. Mol. Liq. 293, 111442 https://doi.org/10.1016/j.molliq.2019.111442.
- Naz, F., Saeed, K., 2021. Investigation of photocatalytic behavior of undoped ZnO and Cr-doped ZnO nanoparticles for the degradation of dye. Inorg. Nano-Metal Chem. 51 (1), 1–11. https://doi.org/10.1080/24701556.2020.1749657.
- Nguyen, S.X., et al., 2019a. Mechanism of enhanced photocatalytic activity of Cr-doped ZnO nanoparticles revealed by photoluminescence emission and electron spin resonance. Semicond. Sci. Technol. 34 (2), 025013 https://doi.org/10.1088/1361-6641/aaf820.
- Nguyen, S.N., et al., 2019b. Investigation on photocatalytic removal of NO under visible light over Cr-doped ZnO nanoparticles. ACS Omega 4 (7), 12853–12859. https://doi. org/10.1021/acsomega.9b01628.
- Nguyen, D.T.C., et al., 2021. Multifunctional ZnO nanoparticles bio-fabricated from Canna indica L. flowers for seed germination, adsorption, and photocatalytic degradation of organic dyes. J. Hazard. Mater. 420, 126586 https://doi.org/ 10.1016/j.jhazmat.2021.126586.
- Nguyen, M.N., et al., 2022. Thermal induced changes of rice straw phytolith in relation to arsenic release: a perspective of rice straw arsenic under open burning. J. Environ. Manage. 304, 114294 https://doi.org/10.1016/j.jenvman.2021.114294.
- Paustian, D., et al., 2022. Sonophotocatalysis—limits and possibilities for synergistic effects. Catalysts 12 (7), 1–12. https://doi.org/10.3390/catal12070754.
- Pavithra, M., Jessie Raj, M.B., 2021. Influence of ultrasonication time on solar light irradiated photocatalytic dye degradability and antibacterial activity of Pb doped ZnO nanocomposites. Ceram. Int. 47 (22), 32324–32331. https://doi.org/10.1016/j. ceramit 2021 08 128
- Pavithra, M., Jessie Raj, M.B., 2022. Synthesis of ultrasonic assisted co-precipitated Ag/ ZnO nanorods and their profound anti-liver cancer and antibacterial properties. Mater. Sci. Eng. B Solid-State Mater. Adv. Technol. 278, 115653 https://doi.org/ 10.1016/j.mseb.2022.115653.
- Pavithra, M., et al., Nov 2023. Zn-doped NiO nanocomposites for efficient solar light-assisted wastewater treatment and its profound for low phytotoxic and antibacterial applications. Plant Nano Biol. 6 (100054) https://doi.org/10.1016/j. plana 2023 100054
- Pneumonia, A.K., et al., 2020. Antibacterial function of chromium nanoparticles against K. Pneumonia, E. coli and P. typhus. Researchsquare 1–7. https://doi.org/10.21203/rs-3-rs-29857/v1
- Qamar, M.A., et al., 2020. Highly efficient g-C3N4/Cr-ZnO nanocomposites with superior photocatalytic and antibacterial activity. J. Photochem. Photobiol. A Chem. 401, 112776 https://doi.org/10.1016/j.jphotochem.2020.112776.
- Qamar, M.A., et al., 2022. Designing and investigation of enhanced photocatalytic and antibacterial properties of 3d (Fe, Co, Ni, Mn and Cr) metal-doped zinc oxide nanoparticles. Opt. Mater. (Amst). 126, 112211 https://doi.org/10.1016/j. optmat.2022.112211.
- Rao, Ś., Shekhawat, G.S., 2014. Toxicity of ZnO engineered nanoparticles and evaluation of their effect on growth, metabolism and tissue specific accumulation in Brassica juncea. J. Environ. Chem. Eng. 2 (1), 105–114. https://doi.org/10.1016/j. iece. 2013.11.029
- Rayani Nivethitha, P., Carolin Jeniba Rachel, D., 2019. A study of antioxidant and antibacterial activity using honey mediated Chromium oxide nanoparticles and its characterization. Mater. Today Proc. 48, 276–281. https://doi.org/10.1016/j. matpr.2020.07.187.
- Rekha, K., et al., 2010. Structural, optical, photocatalytic and antibacterial activity of zinco xide and manganese doped zinc oxide nanoparticles. Phys. B Condens. Matter 405 (15), 3180–3185. https://doi.org/10.1016/j.physb.2010.04.042.
- Ren, G., et al., 2021. Recent advances of photocatalytic application in water treatment: a review. Nanomaterials 11 (7). https://doi.org/10.3390/nano11071804.

- Riaz, N., et al., 2020. Photocatalytic degradation and kinetic modeling of azo dye using bimetallic photocatalysts: effect of synthesis and operational parameters. Environ. Sci. Pollut. Res. 27 (3), 2992–3006. https://doi.org/10.1007/s11356-019-06727-1.
- Rupa, E.J., et al., 2019. Synthesis of a zinc oxide nanoflower photocatalyst from sea buckthorn fruit for degradation of industrial dyes in wastewater treatment. Nanomaterials 9 (12), 1–18. https://doi.org/10.3390/nano9121692.
- Sachin, Jaishree, Singh, N., Singh, R., Shah, K., Pramanik, B.K., 2023. Green synthesis of zinc oxide nanoparticles using lychee peel and its application in anti-bacterial properties and CR dye removal from wastewater. Chemosphere 327, 138497. https://doi.org/10.1016/j.chemosphere.2023.138497.
- Sadeghi Rad, T., et al., 2022. Graphene-based ZnCr layered double hydroxide nanocomposites as bactericidal agents with high sonophotocatalytic performances for degradation of rifampicin. Chemosphere 286 (P2), 131740. https://doi.org/ 10.1016/j.chemosphere.2021.131740.
- Shah, N.I., et al., 2021. Environmentally benign and economical bio-fabrication of ZnO and Cr-doped ZnO nanoparticles using leaf extract of Citrus reticulata for biological activities. Mater. Today Commun. 27, 102383 https://doi.org/10.1016/j.mtcomm.2021.102383.
- Shanmugam, V., Jeyaperumal, K.S., 2018. Investigations of visible light driven Sn and Cu doped ZnO hybrid nanoparticles for photocatalytic performance and antibacterial activity. Appl. Surf. Sci. 449, 617–630. https://doi.org/10.1016/j.apsusc.2017.11.167.
- Sharifi, A., et al., 2022. Application of Cr-doped ZnO for photocatalytic degradation of organic pollutants from aqueous solutions. Int. J. Environ. Sci. Technol. 19 (3), 1507–1518. https://doi.org/10.1007/s13762-021-03290-6.
- Shohany, B.G., Zak, A.K., 2020. Doped ZnO nanostructures with selected elements-structural, morphology and optical properties: a review. Ceram. Int. 46 (5), 5507–5520. https://doi.org/10.1016/j.ceramint.2019.11.051.
- Smječanin, N., et al., August 2022. Algae based green biocomposites for uranium removal from wastewater: kinetic, equilibrium and thermodynamic studies. Mater. Chem. Phys. 283 https://doi.org/10.1016/j.matchemphys.2022.125998.
- Srinet, G., et al., 2020. Room-temperature ferromagnetism on ZnO nanoparticles doped with Cr: an experimental and theoretical analysis. J. Alloys Compd. 849, 156587 https://doi.org/10.1016/j.jallcom.2020.156587.
- Svensson, B.M., et al., 2005. Artemia salina as test organism for assessment of acute toxicity of leachate water from landfills. Environ. Monit. Assess. 102 (1–3), 309–321. https://doi.org/10.1007/s10661-005-6029-z.
- Tangcharoen, T., 2023. Influence of non-magnetic ions doping on structural, morphological, optical, and magnetic properties of nanocrystalline zinc oxide powders. Phys. B Condens. Matter 663, 415010. https://doi.org/10.1016/j. physb.2023.415010.
- Tapia-Salazar, M., et al., 2022. Toxicological effect and enzymatic disorder of non-studied emerging contaminants in Artemia salina model. Toxicol. Reports 9, 210–218. https://doi.org/10.1016/j.toxrep.2022.01.007.
- Ulfa, M., et al., 2023. Hydrothermal effect of gunningite use Pluronic F127-Gelatin as template and the ibuprofen adsorption performance. Heliyon 9 (3), e14473. https://doi.org/10.1016/j.heliyon.2023.e14473.
- Valerio, T.L., et al., 2019. Study of the Nb2O5 insertion in ZnO to dye-sensitized solar cells", material and methods. Mater. Res. 22, 1–5. https://doi.org/10.1590/1980-5373-mr-2018-0864.
- Worku, A.K., et al., 2021. Structural and thermal properties of pure and chromium doped zinc oxide nanoparticles. SN Appl. Sci. 3 (7) https://doi.org/10.1007/s42452-021-04682-6.
- Wu, C., et al., 2011. Solvothermal synthesis of Cr-doped ZnO nanowires with visible light-driven photocatalytic activity. Mater. Lett. 65 (12), 1794–1796. https://doi. org/10.1016/j.matlet.2011.03.070.
- Yan, Z., et al., 2023. The interaction of ZnO nanoparticles, Cr(VI), and microorganisms triggers a novel ROS scavenging strategy to inhibit microbial Cr(VI) reduction. J. Hazard. Mater. 443 (PB), 130375 https://doi.org/10.1016/j. jhazmat.2022.130375.